energy&fuels

pubs.acs.org/EF Article

Structural Dependence of Photogenerated Transformation Products for Aromatic Hydrocarbons Isolated from Petroleum

Sydney F. Niles, Martha L. Chacón-Patiño, Huan Chen, Alan G. Marshall,* and Ryan P. Rodgers*

Cite This: https://doi.org/10.1021/acs.energyfuels.1c02373 Read Online

ACCESS | Metrics & More | Article Recommendations | Supporting Information

ABSTRACT: Previous work has suggested a potential structural dependence for the formation of oil- and water-soluble photoproducts from the simulated solar irradiation of petroleum. Aromatic species in petroleum are thought to play a role in the type and amount of transformation products as a result of their ability to act as chromophores and promote photochemical reactions. To investigate the effect of the aromatic ring number on the formation of photoproducts from petroleum, we subject an Arabian heavy crude oil to a previously developed HPLC-3 method, which fractionates oil based on the number of aromatic rings. All five aromatic ring fractions (1-ring to 5+ rings) produce abundant oil- and water-soluble photoproducts with high oxygen content and similar chemical composition upon photoirradiation in the laboratory, despite large differences in aromaticity in the starting material. The 3- and 4-ring fractions produce the highest amount of dissolved organic carbon, which is quantified by non-purgeable organic carbon analysis. We investigate photoinduced fragmentation, oxidation, and potential polymerization as key processes in the formation of water-solubles from starting material containing different numbers of aromatic rings. As a result of the high amount of sulfur in Arabian heavy crude oil, sulfur-containing photoproducts (O_xS_1) are also investigated.

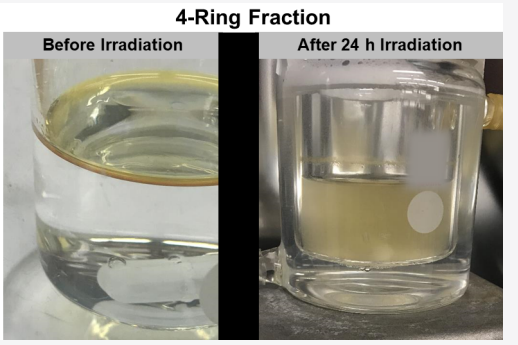

INTRODUCTION

After the *Deepwater Horizon* (DWH) oil spill, which released over 3 million barrels of crude oil into the Gulf of Mexico, the weathering of oil in the environment has been greatly studied.[1−10] Photooxidation has been previously implicated as a dominant process for the formation of oxygenated transformation products; however, additional studies are necessary to determine the chemical processes as well as the structural dependence of photooxidation reactions in petroleum.[1,2,7,10−12] Photochemical reactions can cause oil molecules to become water-soluble upon the addition of oxygen atoms, enabling potentially toxic hydrocarbons to enter waterways and ecosystems, with unknown effects on wildlife and human health.[9,10,13] Thus, understanding these processes and how they change molecular composition and subsequent solubility behavior is of paramount importance.

Recent work has suggested a strong structural dependence for the production of water-soluble photoproducts from petroleum asphaltenes.[9] Asphaltenes are the heptane-insoluble/toluene-soluble portion of crude oil that contains the most aromatic species, which are either single-core (island) or multi-core (archipelago) structural motifs.[14−17] Photoirradiation of fractions enriched in single- and multi-core asphaltenes demonstrated that multi-core species can undergo photo-induced fragmentation to produce water-soluble oxidized polyaromatic hydrocarbons (oxy-PAHs), whereas single-core species do not generate abundant water-solubles.[9] Other studies correlate chemical functionality (e.g., thiophenic versus sulfidic) with the types and abundances of photoproducts observed after solar irradiation, suggesting that functionality also plays a role in photochemical reactions.[8] In addition to photoinduced fragmentation, which was observed for petroleum asphaltenes, polymerization reactions have also been suggested to occur for photooxidized fractions, resulting in higher carbon number species relative to the starting material.[8,9,18]

Chromophores are visible light-absorbing compounds, of which a subset contain polycyclic aromatic hydrocarbons (PAHs), which exist in aromatic fractions of petroleum, such as asphaltenes. They are responsible for initiating photochemical reactions, such as photooxidation and photoinduced fragmentation/polymerization. Two main photooxidation mechanisms are thought to occur in petroleum. The first involves absorption of light by a chromophore, which can react with oxygen to yield a photooxidized product. This reaction is known as direct photooxidation. Conversely, indirect photo-

Special Issue: 2021 Pioneers in Energy Research: Alan Marshall

Received: July 14, 2021
Revised: September 21, 2021

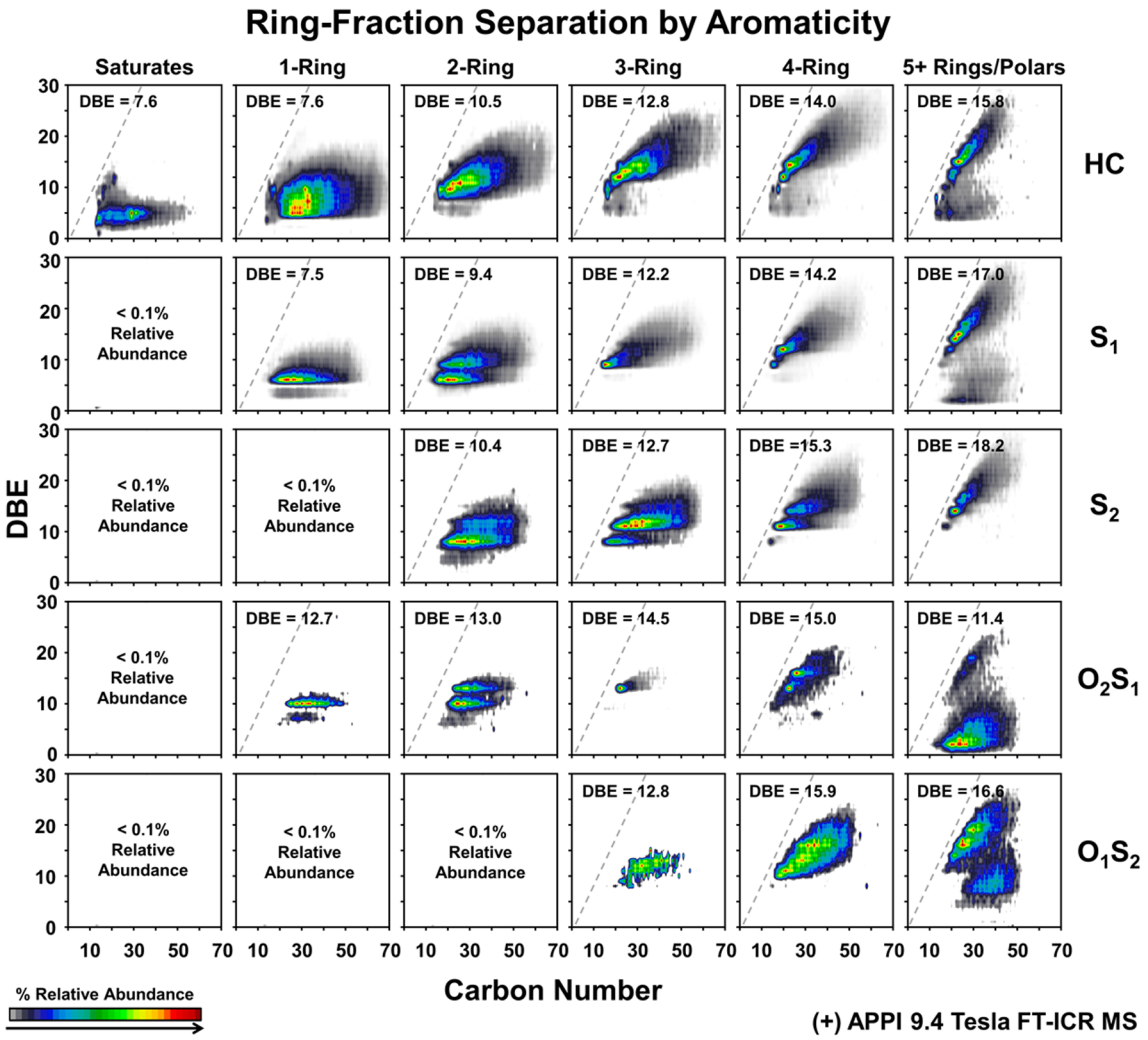

Figure 1. Isoabundance-contoured plots of double bond equivalents (DBE = number of rings plus double bonds to carbon) versus carbon number from (+) APPI FT-ICR MS of ring fractions (saturates, 1 ring, 2 ring, 3 ring, 4 ring, and 5+ ring/polar) isolated from Arabian heavy crude oil. The abundance-weighted DBE values increase with an increasing number of rings.

oxidation can occur when a chromophore absorbs light and then produces reactive oxygen species (e.g., singlet oxygen), which can go on to photooxidize compounds that lack a chromophore, such as alkanes.[1,19−24] It has long been debated whether direct or indirect photooxidation is the dominant mechanism in crude oil. Some studies suggest that, upon addition of β-carotene, singlet oxygen is quenched and photooxidation is inhibited, indicating that singlet oxygen is important for indirect photooxidation of crude oil.[21,23,25] On the other hand, other studies showed that saturated hydrocarbons (which lack chromophores) were resistant to photochemical reactions, whereas alkylated aromatics were found to be the most photochemically active, indicating that direct photooxidation must also occur.[12,26] Thus, we suspect that the number of aromatic rings in a given petroleum compound likely influences which transformation products may form through photooxidation as well as their abundance.

Here, we employ a solar simulator in the laboratory to mimic photooxidation of oil in the environment following a spill. A heavy petroleum sample (chosen due to its high structural and chemical complexity) is subjected to high-performance liquid chromatography (HPLC-3) fractionation to separate compounds by their aromaticity (aromatic ring number).[27] Each fraction (which contains differing numbers of aromatic rings) is irradiated in the solar simulator prior to analysis by Fourier transform ion cyclotron resonance mass spectrometry (FT-ICR MS), which yields molecular information about the photooxidation products. The ultrahigh mass resolution and mass measurement accuracy enable assignment of molecular formulas for confident identification of the transformation products and reveal the effect of the structure for photooxidation processes in the environment. Moreover, non-purgeable organic carbon (NPOC) analysis provides quantification of the amount of water solubles produced from each aromatic ring fraction.

EXPERIMENTAL SECTION

Oil Samples. Arabian heavy crude oil was provided by General Electric Global Research.[28] All solvents were HPLC-grade from J.T. Baker Chemicals (Phillipsburg, PA, U.S.A.) and used as received: heptane (Hep), acetonitrile (ACN), acetone (ACE), toluene (Tol), dichloromethane (DCM), water, cyclohexane, and methanol (MeOH).

HPLC-3 Ring Fraction Separation. Arabian heavy crude oil was subjected to a previously developed HPLC method, which fractionates compounds based on their aromatic ring number.[27] Briefly, the sample was separated on a semi-preparatory-scale, modified

https://doi.org/10.1021/acs.energyfuels.1c02373
Energy Fuels XXXX, XXX, XXX−XXX

Waters Alliance e2695 separations module that features 2 Rheodyne MXT 715-000 6-port, 2-position actuated valves for column switching. The two columns consisted of a Chromegabond dinitroanilinopropyl (DNAP, 10 × 250 mm, 5 μm, ES Industries, West Berlin, NJ, U.S.A.) and a Spherisorb strong cation-exchange (SCX, 10 × 250 mm, 5 μm) column (Waters Corp., Milford, MA, U.S.A.). The SCX column was converted to Ag-SCX by flushing the column with a solution of 30 mg/mL $AgNO_3$ in acetonitrile followed by rinses with acetonitrile, DCM, and hexane before use. A volume of 100 μL of 250 mg of crude oil/mL of toluene was injected onto the column. The seven fractions were collected in preweighed vials and desolvated with dry N_2 gas. Approximately 20 HPLC runs were required to isolate sufficient material for the photooxidation experiments.

Solar Simulation Microcosm. A thin film of oil was generated by adding 20 mg of oil (from each of the resultant ring fractions) dissolved in 50 μL of cyclohexane onto 25 mL of HPLC-grade water in a jacketed beaker. The beaker was left uncovered to allow cyclohexane to evaporate (~2 h). The beaker was attached to a water chiller, placed into a solar simulator (ATLAS Suntest CPS+, ATLAS Material Technology LLC, Chicago, IL, U.S.A.) that produces ~750 W/m (300−800 nm, equivalent to 4 days of natural sunlight per 24 h irradiation time period), and irradiated under an air atmosphere for 24 h at 25 °C. After irradiation, the water-soluble portion was isolated by pipet and filtered with filter paper (120 μm) and a 0.45 μm nylon filter to ensure that no oil-soluble "flakes" were in the water-soluble fractions. The oil layer was isolated by pipet, dried under nitrogen gas, and stored in the dark (4 °C) prior to mass analysis.

Isolation of Water-Soluble Organics. A portion (~5 mL) of the water-soluble fraction was subjected to a solid-phase extraction (SPE) priority pollutant (PPL) extraction method as previously described to isolate water-soluble organic species for FT-ICR MS analysis.[29] Another portion (~20 mL) of the water was stored for NPOC analysis. Prior to PPL extraction, water samples were acidified to pH 2 with concentrated hydrochloric acid. The stationary phase of a PPL cartridge was then conditioned with methanol, and the acidified water samples were loaded for the extraction of water-solubles. Acidified water was added to rinse the SPE column and remove any salts. After overnight drying, methanol was added to elute water-soluble hydrocarbons, and the extracts were infused into the mass spectrometer without further modification or dilution.

NPOC Analysis. NPOC measurement of filtered water samples was conducted with a Shimadzu TOC-L instrument as previously described.[18]

FT-ICR MS Analysis. Mass analysis of virgin (unirradiated) ring fractions and resultant water- and oil-soluble photoproducts was conducted with a custom-built 9.4 T FT-ICR mass spectrometer.[30] The oil-soluble fraction was dissolved in toluene to a concentration of 150 μg/mL for ionization by positive-ion (+) atmospheric pressure photoionization (APPI) before and after solar irradiation as previously described.[31] The oil-soluble fractions were also analyzed by (+)/(−) electrospray ionization (ESI); fractions were reconstituted in toluene and dissolved with methanol to a final concentration of 150 μg/mL in Tol/MeOH (1:1) as described elsewhere.[7,8] For (+) ESI analysis, oil-soluble fractions were acidified with formic acid to a concentration of 2% formic acid (v/v) to ionize ketone/aldehyde species as previously described.[5,7,8] For (−) ESI analysis, tetramethylammonium hydroxide (TMAH) base was added 0.25% (v/v) to promote ionization of acidic species.[32] Following PPL extraction, water-soluble extracts were infused directly into the mass spectrometer at 0.5 μL/min for (−) ESI FT-ICR MS analysis as previously described.[33] Predator and PetroOrg software were used for molecular formula assignments.[34,35]

RESULTS AND DISCUSSION

Ring Fraction Separation. The HPLC-3 fractionation method effectively separates Arabian heavy crude oil according to the number of aromatic rings in a compound, as illustrated by the isoabundance-contoured plots of double bond equivalents (DBE = number of rings plus double bonds to carbon) versus carbon number from (+) APPI FT-ICR MS analysis of the ring fractions in Figure 1. APPI is an effective means to reveal differences in aromaticity due to its ability to ionize nonpolar aromatic compounds. Thus, it is employed to illustrate separation of the oil into its corresponding aromatic ring fractions. The saturates fraction exhibits low heteroatom content and presents low aromaticity (majority of species have DBE values of <10) for the hydrocarbon (HC) class, which is expected for more saturated hydrocarbons (cycloalkanes). Furthermore, its low heteroatom content is shown in Figure S1 of the Supporting Information, which displays the heteroatom compound class distribution from (+) APPI analysis of the parent ring fractions; the saturates fraction contains only HC and O_x compounds (most likely as a result of oxidation products that are unavoidable in APPI). All six ring fractions exhibit high relative abundances of HC; the DBE versus carbon number plots in Figure 1 show clear separation by aromaticity for HC compounds in the 1- to 5-ring fractions. Specifically, as the number of aromatic rings increases (from left to right), the compositional range shifts to higher abundance-weighted DBE values, and the compositional range of the compounds shifts closer to the planar PAH limit, which is shown by a gray dotted line.[36] Moreover, the ring fractions are shown to contain different compound classes, specifically, O_xS_1 species and nitrogen-containing compounds (e.g., N_1S_1 and N_1O_x) that elute primarily in the 5-ring/polar fraction (Figure S1 of the Supporting Information).

Sulfur chemistry has been identified as an important aspect of petroleum photochemistry; sulfidic and thiophenic compounds isolated from an Arabian crude oil distillate demonstrated the production of abundant water-soluble SO_x compounds, which may be potentially toxic.[8] Thiophenic compounds from an Arabian heavy distillate cut were shown to produce abundant water-soluble O_xS_1 species (up to $O_{18}S_1$), whereas the sulfidic species produced lower oxygenated species (up to O_7S_1). Moreover, the thiophenes underwent photo-induced polymerization upon irradiation, which increased the aromaticity and carbon number of the photoproducts. In another study, abundant SO_x compounds were produced upon photoirradiation of a petroleum-derived asphalt binder, which contained high amounts of S_1 and S_2 prior to irradiation.[18] Similarly, the S_1 and S_2 classes present high relative abundance for the 1- to 5-ring fractions, and they exhibit a progressive shift to higher DBE values as the ring number increases. The classes also exhibit relative maxima at DBE values corresponding to aromatic sulfur cores. For example, S_1 compounds in 1- to 4-ring fractions exhibit relative maxima at DBE of 6, 9, and 12, which correspond to benzothiophene, dibenzothiophene, and benzonaphthothiophene cores with varying degrees of alkylation. The S_2 class contains compounds with higher relative abundance at DBE of 8, 11, and 14, which suggests the presence of aromatic sulfur cores that contain two sulfur atoms, such as cycloalkyl/alkyl-substituted versions of benzodithiophene. As a result of the known photoreactivity of thiophene cores, as demonstrated for a similar study on an Arabian heavy distillate, these species are of interest for the current study.[8]

The ring fractions also contain notable amounts of O_xS_y compounds, which increase in relative abundance with an increasing ring number, as shown in Figure S1 of the Supporting Information. The O_2S_1 class generally demonstrates an increase in aromaticity with an increasing ring number for 1- to 4-ring fractions. However, the 5+ ring/polar fraction contains O_2S_1 compounds with low aromaticity (as

https://doi.org/10.1021/acs.energyfuels.1c02373
Energy Fuels XXXX, XXX, XXX−XXX

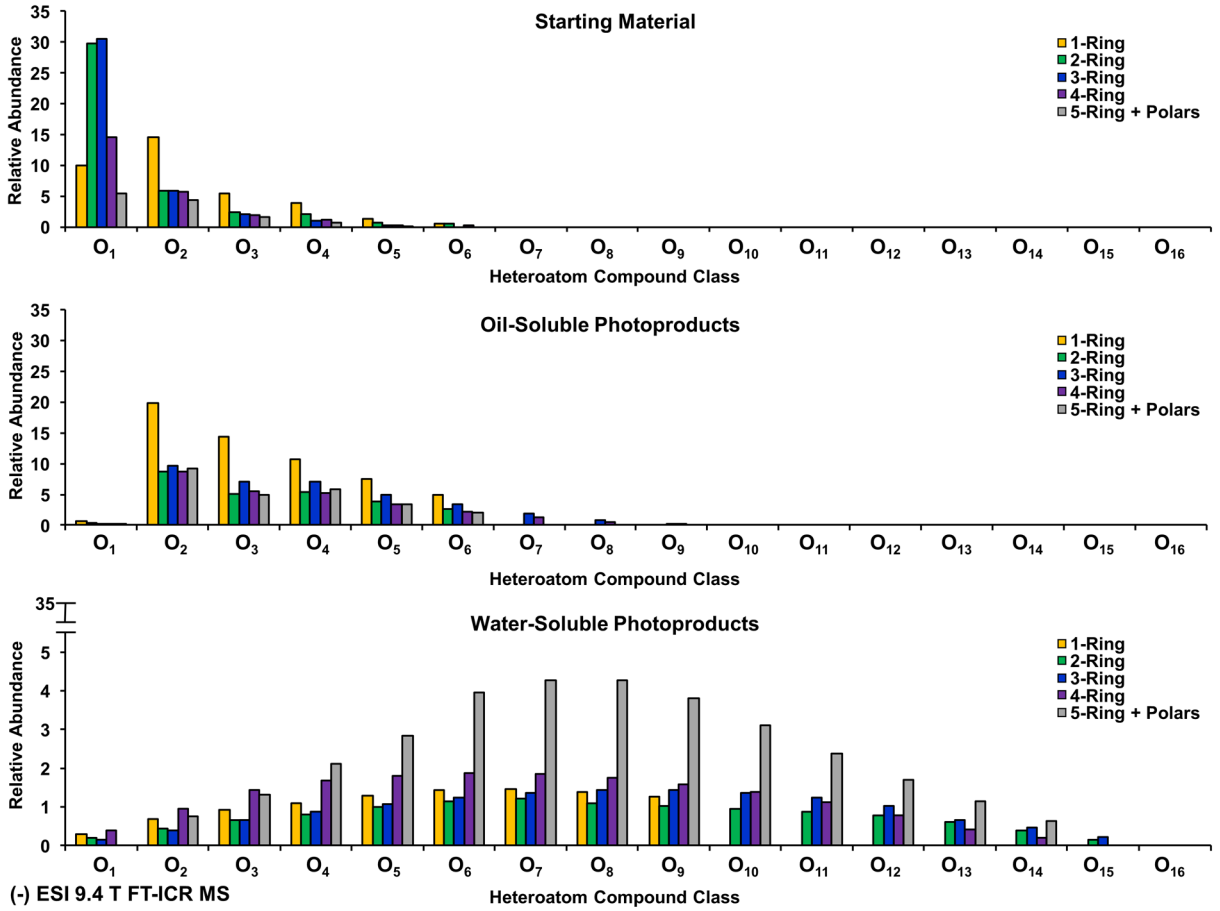

Figure 2. Heteroatom compound class distributions for the O_x class from (−) ESI FT-ICR MS analysis of virgin ring fractions and their resultant oil- and water-soluble photoproducts.

low as DBE of 2) in addition to compounds near the PAH limit, likely indicating co-elution of highly aromatic species with low-aromaticity compounds that elute in the final fraction as a result of their polar functionality. The O_1S_2 compounds demonstrate a similar trend; the 5+ ring/polar fraction contains O_1S_2 species, which exhibit a bimodal distribution. Unlike the O_2S_1 class, the O_1S_2 class for the 5+ ring/polar fraction has a higher relative abundance of aromatic compounds than the low-aromaticity species. It is important to note that the final fraction contains not only compounds with 5 or more rings but also compounds with high polarizability (e.g., O_xS_y species), which interact strongly with the stationary phase as a result of the heteroatom content rather than aromaticity. Thus, the low-DBE species in those classes elute in the 5+ ring/polar fractions as a result of their polarity and not their aromatic ring number.

Photooxidation of Ring Fractions. Ring fractions were analyzed by (−) ESI FT-ICR MS before and after laboratory irradiation to target acidic functionalities, which are produced upon photooxidation of crude oil.[5] Previous analysis of photooxidized petroleum by (−) ESI FT-ICR MS revealed the presence of oil-soluble acidic species with 1−9 oxygen atoms (e.g., O_1−O_9).[5,8,9,18,37] Water-soluble fractions from photoirradiated petroleum were shown to contain highly oxidized species (up to O_{19}).[8,9,18,37] The heteroatom compound class distribution for O_x species is shown in Figure 2 for the (−) ESI FT-ICR MS analysis of the starting material (top panel), oil-soluble photoproducts (middle panel), and water-soluble photoproducts (bottom panel) for all ring fractions. The virgin aromatic ring fractions show appreciable amounts of "preoxidized" species, such as O_1−O_5, which are present for all ring fractions prior to irradiation. The most abundant O_x species are O_1 and O_2 compounds, and higher oxygenated O_x species (>O_6) are not observed for the 1- to 5-ring fractions. As a result of extensive separations required to collect adequate amounts of each ring fraction for photooxidation experiments, we suspect that low levels of oxidation occurred in sample preparation (e.g., O_1 and O_2 classes, discussed below).

Following laboratory irradiation, the oil-soluble photoproducts (middle panel in Figure 2) for 1-, 2-, 3-, 4-, and 5+ ring/polar fractions exhibit higher abundances of more highly oxygenated compounds (e.g., O_5 and O_6), with a concurrent drop in the relative abundance of the O_1 (preoxidized) species. The established ionization efficiency differences between alcohols (O_1 class, low efficiency) and carboxylic acids (O_2 class, high efficiency) indicate the generation of oil-soluble, acidic photoproducts (>O_2). An oil layer was not present after irradiation of the 3- and 4-ring fractions; instead, particulates formed in the water after irradiation and were subsequently determined to be toluene-soluble. Thus, the particulates that were water-insoluble and suspended in the water were isolated, analyzed, and classified as oil-soluble photoproducts. The oil-soluble 3- and 4-ring photoproducts contain more highly oxygenated compounds (e.g., O_7−O_9) than the other ring fractions. Conversely, the 1-, 2-, and 5-ring fractions produced

https://doi.org/10.1021/acs.energyfuels.1c02373
Energy Fuels XXXX, XXX, XXX−XXX

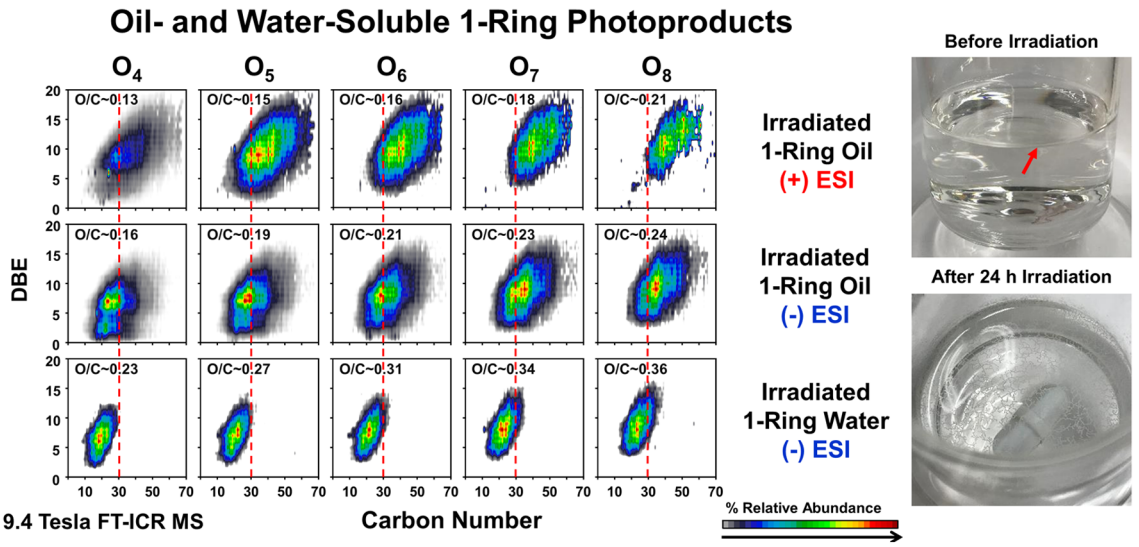

Figure 3. Isoabundance-contoured plots of DBE versus carbon number from (+/−) ESI FT-ICR MS analysis of 1-ring oil- and water-soluble photoproducts after 24 h of irradiation. The right panel shows photos of the 1-ring fraction as a thin film of oil on water prior to irradiation (top) and after 24 h of irradiation (bottom).

higher abundances of lower oxygenated O_x species (e.g., O_2−O_4) relative to the starting material.

Water-soluble photoproducts from the ring fractions were isolated by PPL extraction and analyzed by (−) ESI FT-ICR MS to reveal abundant O_x compounds in water-soluble extracts from all five aromatic ring fractions; the heteroatom compound class distributions are shown in the bottom panel of Figure 2. The relative abundances of the O_x compounds from the water-soluble extracts present pseudo-Gaussian distributions from ~O_1−O_{16}, which are typical for water solubles produced from photooxidized petroleum.[8,9,18,37]

As noted above, we also subjected the saturates fraction to photoirradiation, and the oil-soluble photoproducts were characterized by FT-ICR MS. We hypothesize that saturates, which do not contain abundant chromophores (aromatic rings), are unable to absorb light to promote photooxidation. The DBE versus carbon number plots and heteroatom compound class distribution from (−)/(+) ESI FT-ICR MS analysis of the saturates before and after irradiation are displayed in Figure S2 of the Supporting Information and suggest that the oil-soluble O_x photoproducts are chemically similar to the starting material; the compositional range of the O_x species is nearly identical before and after photoirradiation for both ionization modes. Moreover, the heteroatom compound class distribution (bottom panel) indicates that the oil-soluble photoproducts exhibit relative abundances of O_x similar to the starting material and suggests that saturates do not photooxidize extensively. Finally, it is important to keep in mind that the saturates fraction shows extremely low abundances of heteroatoms (Figure S1 of the Supporting Information), and any oxygen-containing functionalities (e.g., carboxylic acids) will ionize preferentially relative to saturated hydrocarbons by ESI. Thus, as a result of their similarity to the starting material, low abundance, and inability to differentiate any compositional differences in the photoirradiated products from potential low levels of preoxidation, we shall not focus on these results.

Mass analysis of the starting material and oil-soluble photoproducts was also conducted by use of (+) ESI, and the heteroatom compound class distributions are shown in Figure S3 of the Supporting Information. The oil-soluble photoproducts contain a continuum of oxygenated species detected by (+) ESI, in agreement with previous reports that both ketone/aldehyde species (accessed by (+) ESI) as well as acidic/alcohol/hydroxyl species (accessed by (−) ESI) are formed through photooxidation of petroleum. All ring fractions contain oil-soluble O_x, O_xS_1, and N_1O_x species upon photoirradiation; however, their relative abundances vary according to ring number. The 1-ring fraction produces high amounts of O_x after photooxidation. Conversely, the 2- and 3-ring fractions produce high amounts of O_xS_1 upon irradiation. Finally, the 4- and 5-ring fractions produce elevated levels of both O_xS_1 and N_1O_x classes.

Figure 3 presents isoabundance-contoured plots of DBE versus carbon number for the oil- and water-soluble photoproducts from 24 h irradiation of the 1-ring fraction, analyzed by (+) and (−) ESI. The (+) ESI O_x species appear to be more alkylated (higher carbon number) than those ionized by (−) ESI, especially for the O_5 and O_6 compounds; this trend is reflected in the lower abundance-weighted O/C ratios for the (+) ESI species than the (−) ESI oil-soluble classes. The compositional range of the O_x compounds shifts to a higher carbon number with an increased oxygen content (e.g., from O_4 to O_8) for both ionization modes, as illustrated by a dotted red line, and higher O/C ratios for higher oxygenated compounds (e.g., O_8). Furthermore, the (+) APPI analysis of the starting material (top panels of Figure 1) reveals that the majority of the HC compounds in the 1-ring fraction have DBE of <15, over a wide carbon number range (10 < carbon number < 70), which yields a "flat", relatively uniform, horizontal distribution in compositional space; conversely, the oil-soluble photoproducts shift to higher DBE (up to 20) with an increasing carbon number, to yield a "tilted" compositional space. Such a trend would be consistent with the preferential incorporation of oxygen in forms that have a double bond to carbon (aldehyde, ketone, esters, and carboxylic acid) that would yield a DBE increase of 1. However, photoinduced polymerization[18] of lower carbon number species could also

https://doi.org/10.1021/acs.energyfuels.1c02373
Energy Fuels XXXX, XXX, XXX−XXX

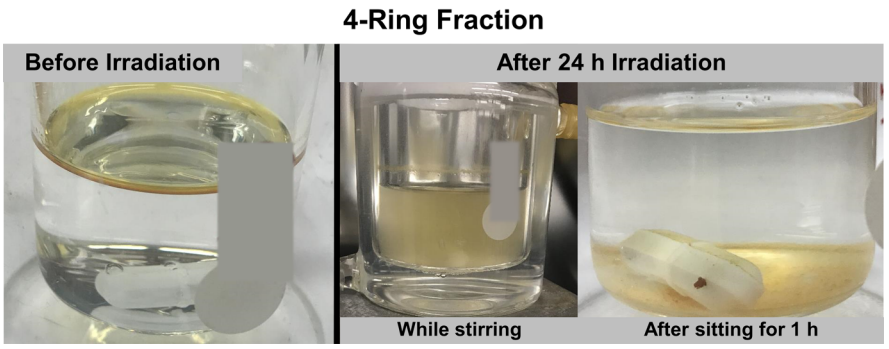

Figure 4. Photos of the 4-ring fraction before irradiation (left), immediately after irradiation (middle), and 1 h after irradiation (right).

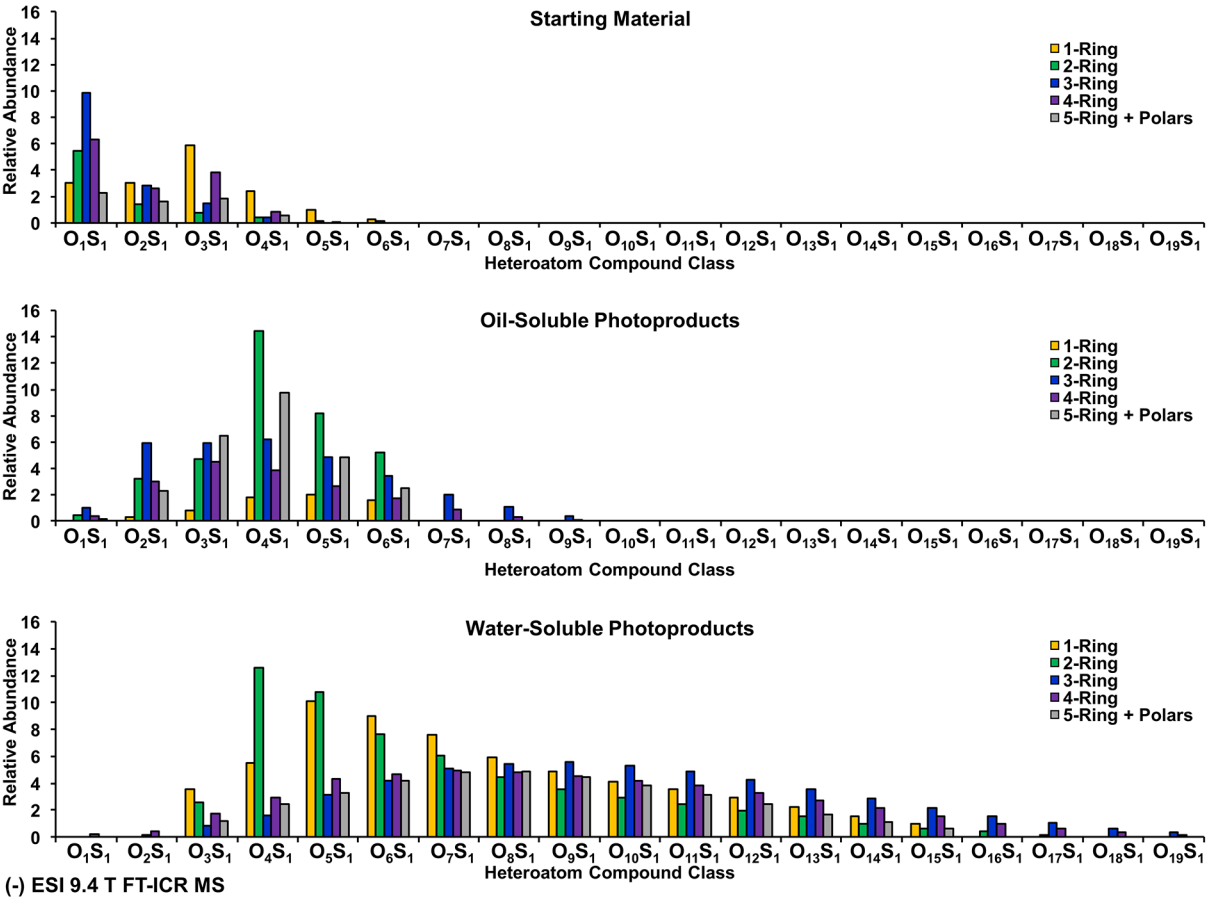

Figure 5. Heteroatom compound class distributions from (−) ESI FT-ICR MS analysis of the water-soluble extracts from 24 h irradiated ring fractions, displayed for the O_x class (top) and O_xS_1 class (bottom).

explain the observed trends. Thus, future experiments will focus on the removal of water-soluble photooxidation products as they are formed to further investigate their effect on the composition of the water-soluble products.

The oil-soluble extract was analyzed by (−) ESI to reveal abundant O_x compounds from O_1−O_9, as seen in Figure 2 (class graph), and the isoabundance-contoured plots of DBE versus carbon number for O_4−O_8 compounds, displayed in Figure 3, reveal that water-soluble O_x photoproducts occupy a lower carbon number range (<30) than the oil-soluble photoproducts. The red dotted line illustrates the difference in carbon number ranges between oil- and water-soluble compounds; we hypothesize that lower-carbon number compounds with the same number of oxygen atoms are transferred to the water layer as a result of their higher O/C ratio. This phenomenon is shown by the higher abundance-weighted O/C ratios for the water-soluble species than their oil-soluble counterparts. Such a trend has been previously reported in petroleum photooxidation studies.[8,18,37]

The right panel of Figure 3 shows photos of the 1-ring fraction as a thin layer of oil (red arrow) on the water before (top) and after (bottom) 24 h of irradiation in the solar simulator and reveals visual changes to the oil layer after irradiation. The exact reason behind the "clumping" of the surface film is currently unknown but is most likely linked to the increased levels of oil-soluble photooxidation products with polar oxygen functionalities. The 4-ring fraction also showed dramatic physical changes after solar irradiation; Figure 4

https://doi.org/10.1021/acs.energyfuels.1c02373
Energy Fuels XXXX, XXX, XXX−XXX

displays photos of the oil before and after irradiation and illustrates the generation of water-soluble compounds produced after irradiation. Unlike the 1-ring fraction (Figure 3), the 4-ring oil film is completely disrupted after solar irradiation, and particulates have formed (middle panel of Figure 4) to yield turbid water. Following irradiation, the sample was allowed to sit for 1 h, and the particulates fell to the bottom as a result of their higher density (right panel of Figure 4).

Production of SO_x Species from Photooxidation. Sulfur-containing compounds (S_1 and O_xS_1) are present in high abundance in the starting material for the ring fractions (Figure S1 of the Supporting Information); as previously noted, those species have been shown to produce oxygenated O_xS_y compounds upon photooxidation of road asphalt and petroleum.[8,18] Before irradiation of the ring fractions, (−) ESI FT-ICR MS analysis of the starting material reveals appreciable amounts of O_xS_1 species with up to six oxygen atoms, as shown by the heteroatom plots in Figure 5. However, following irradiation, the distribution of O_xS_1 compounds in the oil-soluble extract exhibits a pseudo-Gaussian distribution and shifts to a higher oxygen number centered around O_4S_1. The 2-ring fraction produces the highest abundance of O_4S_1 species in the oil-soluble photoproducts, in agreement with its high S_1 content in the starting material, most likely in the form of benzothiophene cores. Furthermore, all of the ring fractions produce notable amounts of O_xS_1 compounds in the water; however, they do not all present the same distribution. The 1- and 2-ring fractions contain the highest abundance of O_4S_1 and O_5S_1 compounds, with lower abundance of higher oxygenated species (e.g., $O_{15}S_1$). Conversely, the 3-, 4-, and 5-ring fractions present a pseudo-Gaussian distribution centered around O_9S_1. Moreover, the 3- and 4-ring fractions extend to the most oxygenated species (up to $O_{19}S_1$).

NPOC Analysis of Water. Following filtration of the water-soluble extracts from irradiated ring fractions, the 3- and 4-ring fractions exhibited a yellow color, suggesting that a high proportion of oil was transferred to the water after photo-irradiation, as seen in Figure 6. Therefore, we subjected water-soluble photoproducts to NPOC quantification to yield information regarding the mass transfer of oil to water after photooxidation. Although mass spectrometry reveals the molecular composition of the water, it is not quantitative due to differences in ionization efficiency for different components. The NPOC values for the water-soluble extracts from the irradiated ring fractions are displayed in Figure 6 and suggest that the 3- and 4-ring fractions yield the highest proportion of water-soluble material upon photooxidation, whereas the other fractions produce lower amounts of water-soluble photoproducts. Triplicate measurements yielded error values between 0.02 mg/L (lowest concentration) and 0.55 mg/L (highest concentration) for the range of concentrations analyzed (13−150 mg/L).

Molecular Composition of Water-Soluble Photoproducts. The water-soluble species have higher oxygen content relative to the starting material and oil-soluble photoproducts, as shown by the heteroatom compound class distributions in Figures 2 and 5. The heteroatom compound class distributions for the O_x and O_xS_1 species from the water-soluble extracts of irradiated ring fractions are shown in Figure S4 of the Supporting Information. The bottom panel of Figure 6 shows that the lower aromaticity fractions (1 and 2 ring) have higher relative abundance of lower oxygenated O_xS_1 photoproducts, (e.g., O_4S_1), whereas the higher aromaticity compounds (3, 4, and 5+ ring/polar) exhibit higher abundance of higher oxygenated species (e.g., $O_{12}S_1$−$O_{17}S_1$).

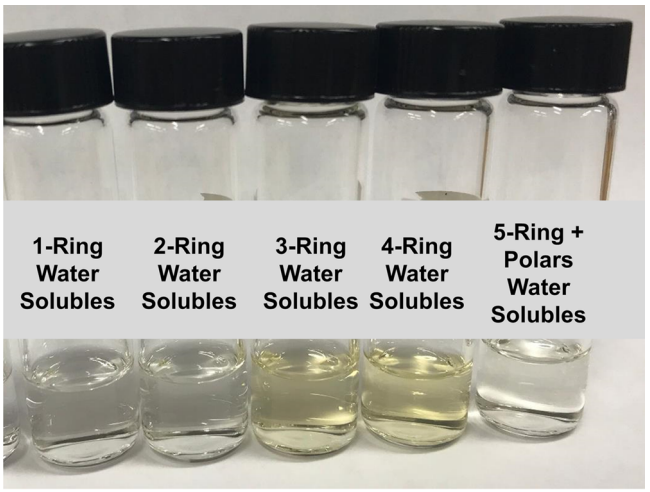

Sample	NPOC (mg / L)
1-ring water 24h	74.3
2-ring water 24 h	48.2
3-ring water 24 h	150.6
4-ring water 24h	83.1
5-ring water 24h	13.5

Figure 6. Water-soluble extracts from ring fractions after 24 h of irradiation (top), showing the abundance of water solubles produced by the 3- and 4-ring fractions. The NPOC and total nitrogen values of the water are displayed for the ring fractions in the table (bottom).

As previously demonstrated in Figure 3, the water- and oil-soluble photoproducts occupy complementary compositional ranges, with the water-soluble species displaced to lower carbon numbers. Figure 7 presents the DBE versus carbon number plots for the 1- and 2-ring fractions before irradiation [(+) APPI, left] and after irradiation [(−) ESI, right] and highlights differences in carbon number ranges between oil- and water-soluble photoproducts relative to their HC and O_1 precursors. Similar trends were noted for all water-soluble O_x classes. For example, the water-soluble O_7 classes are comprised of lower carbon number species (<35 carbons) than their oil-soluble counterparts, which contain up to ∼60 carbon atoms. The compositional range for the water-soluble species is traced in red to illustrate differences between the oil- and water-soluble fractions.

The isoabundance-contoured plots of DBE versus carbon number from (−) ESI FT-ICR MS analysis of the water-soluble extracts are shown in Figure 8 and are grouped by oxygen content (O_1−O_4, O_5−O_8, and O_{9+}). A comparison of lower oxygenated compounds (O_1−O_4), mid-oxygenated compounds (O_5−O_8), and higher oxygenated compounds (O_{9+}) highlights differences in compositional ranges for water-soluble species as a function of the increasing oxygen content. Surprisingly, despite clear differences in aromaticity in the starting material (Figure 1), all five aromatic ring fractions generally produce similar water-soluble photoproducts. However, some notable differences can be observed between fractions; as the aromatic ring number increases, the composition of the O_x compounds shifts slightly upward in DBE and toward the PAH limit (gray dotted line), which correlates with previously established compositional differ-

https://doi.org/10.1021/acs.energyfuels.1c02373
Energy Fuels XXXX, XXX, XXX−XXX

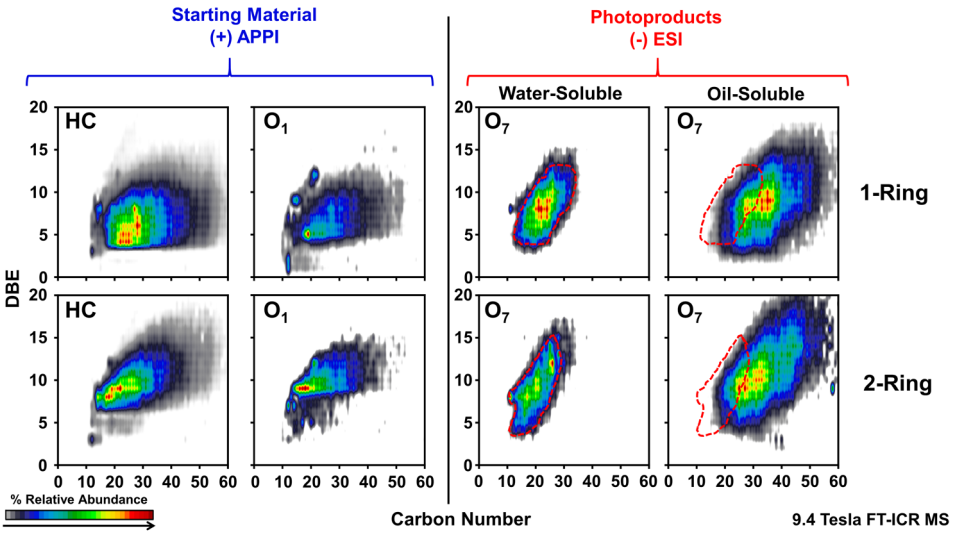

Figure 7. Isoabundance-contoured plots of DBE versus carbon number from (+) APPI analysis of the starting material (left) and (−) ESI of the oil- and water-soluble extracts (right), illustrating differences in the compositional range for water- and oil-soluble O_7 photoproducts and suggesting potential starting material for the photoproducts.

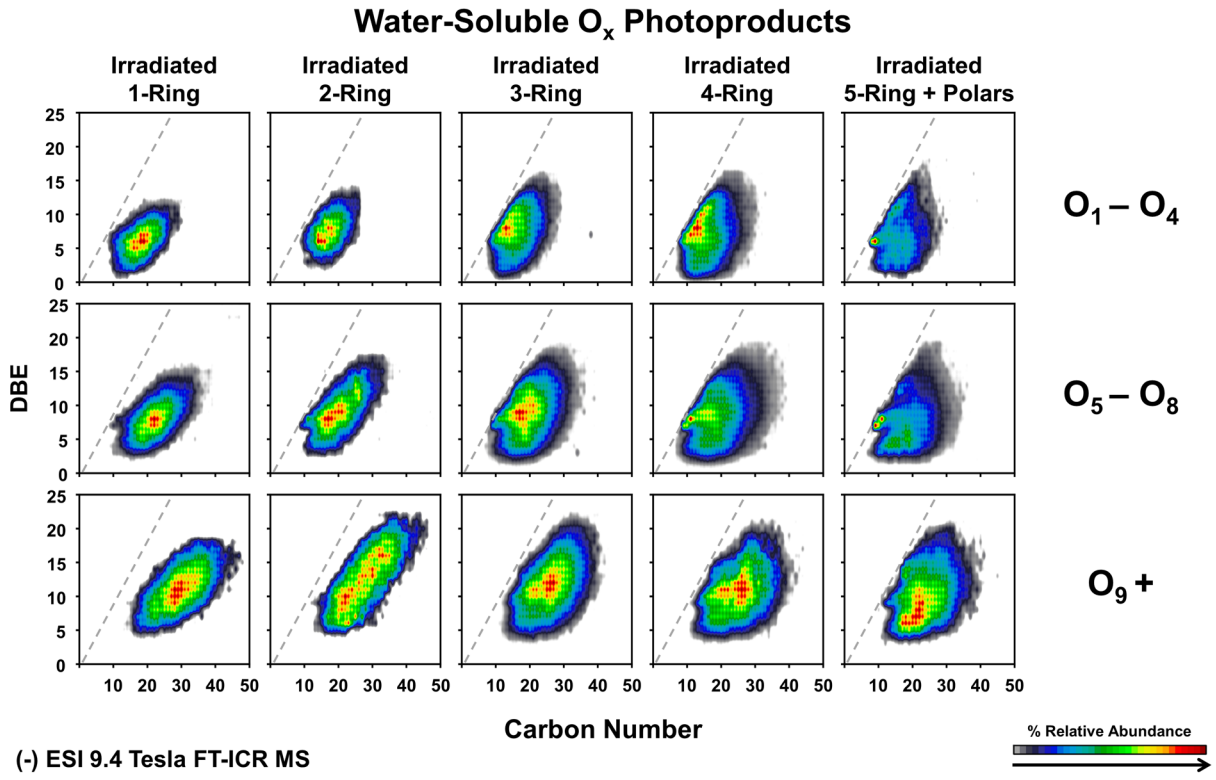

Figure 8. Isoabundance-contoured plots of DBE versus carbon number from (−) ESI FT-ICR MS analysis of the ring fractions are displayed for low-oxygenated species (O_1−O_4, top), medium-oxygenated species (O_5−O_8, middle), and high-oxygenated species (O_{9+}, bottom).

ences in the starting material (Figure 1). The low-DBE photooxidation products in the 3-, 4-, and 5-ring fractions (upper right panel of Figure 8) strongly suggest photofragmentation reactions of higher carbon number species as well as archipelago species that contain multiple aromatic cores, which yield low DBE products. Specifically, the water-soluble extract contains species with DBE of 1 for the O_1−O_4 classes, which could be formed by photooxidation and subsequent dealkylation of higher carbon number species, whereas the starting material contained compounds with higher aromaticity (DBE of >10). Furthermore, the most prominent low-DBE species begin in the 3-ring fraction and continue into the 4- and 5-ring/polar; previous work has identified archipelago maltenes in this compositional range.[31]

Finally, the carbon number restriction imposed by water-solubility and its relationship with oxygen content are clearly evident in Figure 8. Lower oxygenated compounds (O_1−O_4) are limited to carbon numbers below 30, which slightly

https://doi.org/10.1021/acs.energyfuels.1c02373
Energy Fuels XXXX, XXX, XXX−XXX

increase to 35 for mid-oxygenated compounds (O_5−O_8) and end with higher oxygenated compounds (O_{9+}) at ∼40. Higher carbon number photoproducts with similar oxygen content remain oil-soluble, as illustrated in Figure 3. Thus, photochemistry contributes to both oxidative and fragmentation reactions that favor the production of water-soluble species with similar compositions (DBE and carbon number ranges) despite different starting materials. As discussed earlier, the influence of photoinduced polymerization (recently demonstrated)[9] on photoproducts will be the subject of future research. However, the relative abundance of those species varies based on the structure and functionality.

Conclusions and Future Directions. In summary, a HPLC method fractionates oil based on the number of aromatic rings, which enables separate photoirradiation microcosm experiments and analysis of the water-soluble photoproducts for fractions enriched in differing numbers of aromatic rings (1- to 5+ rings). The aromatic ring fractions were demonstrated to undergo photooxidation and photofragmentation to produce abundant oxygenated photoproducts, such as O_x and O_xS_y, upon laboratory irradiation. The analysis of water-solubles suggests that similar photoproducts are formed from all of the aromatic ring fractions, despite different starting materials; such behavior is not unexpected given the recent confirmation of both abundant single- and multi-core aromatics in petroleum. However, the amount of water-soluble organic material generated and heteroatom content varies between fractions as well as their proximity to the planar PAH limit (higher number of aromatic rings yields water-soluble products that lie closer to the PAH line). Specifically, after irradiation, the 3- and 4-ring fractions produced yellow water, the oil layer was disrupted, high amounts of NPOC were detected (up to 150.6 mg/L for the 3-ring fraction), and the water-soluble species were closest to the PAH limit. Finally, the ring fractionation data support previous carbon number and oxygen content trends that suggest that a higher number of oxygens is required to make higher carbon number species water-soluble. Future work to decouple the potential contributions of high-molecular-weight species that contribute to lower molecular weight water-solubles (photofragmentation) from that of lower molecular weight species (photooxidation and potentially photopolymerization) would require extensive ring fractionation of a series of distillate cuts. Given the effort required to isolate sufficient amounts of each ring fraction for microcosm, mass spectrometry, and NPOC analysis described herein, such experiments are currently impractical.

■ ASSOCIATED CONTENT

Supporting Information

The Supporting Information is available free of charge at https://pubs.acs.org/doi/10.1021/acs.energyfuels.1c02373.

Heteroatom compound class distribution from (+) APPI FT-ICR MS analysis of virgin ring fractions (Figure S1), DBE versus carbon number plots and heteroatom compound class distribution for virgin and 24 h irradiated saturated hydrocarbons (Figure S2), heteroatom compound class distribution from (+) ESI FT-ICR MS analysis of virgin and 24 h irradiated aromatic ring fractions (Figure S3), and heteroatom compound class distribution from (−) ESI FT-ICR MS analysis of water-soluble SO_x and O_x photoproducts (Figure S4) (PDF)

■ AUTHOR INFORMATION

Corresponding Authors

Alan G. Marshall − *Department of Chemistry and Biochemistry, Florida State University, Tallahassee, Florida 32306, United States; Ion Cyclotron Resonance Program, National High Magnetic Field Laboratory, Florida State University, Tallahassee, Florida 32310, United States;* orcid.org/0000-0001-9375-2532; Phone: +1-850-644-0529; Email: marshall@magnet.fsu.edu; Fax: +1-850-644-1366

Ryan P. Rodgers − *Department of Chemistry and Biochemistry, Florida State University, Tallahassee, Florida 32306, United States; Ion Cyclotron Resonance Program, National High Magnetic Field Laboratory, Florida State University, Tallahassee, Florida 32310, United States;* orcid.org/0000-0003-1302-2850; Phone: +1-850-644-2398; Email: rodgers@magnet.fsu.edu; Fax: +1-850-644-1366

Authors

Sydney F. Niles − *Department of Chemistry and Biochemistry, Florida State University, Tallahassee, Florida 32306, United States; Ion Cyclotron Resonance Program, National High Magnetic Field Laboratory, Florida State University, Tallahassee, Florida 32310, United States;* orcid.org/0000-0002-3487-6612

Martha L. Chacón-Patiño − *Ion Cyclotron Resonance Program, National High Magnetic Field Laboratory, Florida State University, Tallahassee, Florida 32310, United States;* orcid.org/0000-0002-7273-5343

Huan Chen − *Ion Cyclotron Resonance Program, National High Magnetic Field Laboratory, Florida State University, Tallahassee, Florida 32310, United States;* orcid.org/0000-0002-6032-6569

Complete contact information is available at: https://pubs.acs.org/10.1021/acs.energyfuels.1c02373

Notes

The authors declare no competing financial interest.

■ ACKNOWLEDGMENTS

The authors thank Steven M. Rowland for HPLC-3 experiments to isolate ring fractions and Amy M. McKenna for assistance with data processing. The authors thank Samuel P. Putnam for NPOC data collection, analysis, and interpretation. This research was made possible in part by a grant from the Gulf of Mexico Research Initiative and in part by the National Science Foundation Division of Chemistry through Cooperative Agreement DMR-1644779, the Florida State University Future Fuels Institute, and the State of Florida. Data are publicly available through the Gulf of Mexico Research Initiative Information & Data Cooperative (GRIIDC) at https://data.gulfresearchinitiative.org (DOI: 10.7266/FY9QWH5F).

■ REFERENCES

(1) Ward, C. P.; Overton, E. B. How the 2010 Deepwater Horizon Spill Reshaped Our Understanding of Crude Oil Photochemical Weathering at Sea: A Past, Present, and Future Perspective. *Environ. Sci. Process. Impacts* **2020**, *22*, 1125.

(2) Ward, C. P.; Sharpless, C. M.; Valentine, D. L.; French-McCay, D. P.; Aeppli, C.; White, H. K.; Rodgers, R. P.; Gosselin, K. M.; Nelson, R. K.; Reddy, C. M. Partial Photochemical Oxidation Was a Dominant Fate of *Deepwater Horizon* Surface Oil. *Environ. Sci. Technol.* **2018**, *52* (4), 1797−1805.
(3) Aeppli, C.; Carmichael, C. A.; Nelson, R. K.; Lemkau, K. L.; Graham, W. M.; Redmond, M. C.; Valentine, D. L.; Reddy, C. M. Oil Weathering after the *Deepwater Horizon* Disaster Led to the Formation of Oxygenated Residues. *Environ. Sci. Technol.* **2012**, *46* (16), 8799−8807.
(4) Kujawinski, E. B.; Reddy, C. M.; Rodgers, R. P.; Thrash, J. C.; Valentine, D. L.; White, H. K. The First Decade of Scientific Insights from the *Deepwater Horizon* Oil Release. *Nat. Rev. Earth Environ.* **2020**, *1*, 237.
(5) Ruddy, B. M.; Huettel, M.; Kostka, J. E.; Lobodin, V. V.; Bythell, B. J.; McKenna, A. M.; Aeppli, C.; Reddy, C. M.; Nelson, R. K.; Marshall, A. G.; Rodgers, R. P. Targeted Petroleomics: Analytical Investigation of Macondo Well Oil Oxidation Products from Pensacola Beach. *Energy Fuels* **2014**, *28* (6), 4043−4050.
(6) Chen, H.; Hou, A.; Corilo, Y. E.; Lin, Q.; Lu, J.; Mendelssohn, I. A.; Zhang, R.; Rodgers, R. P.; McKenna, A. M. 4 Years after the *Deepwater Horizon* Spill: Molecular Transformation of Macondo Well Oil in Louisiana Salt Marsh Sediments Revealed by FT-ICR Mass Spectrometry. *Environ. Sci. Technol.* **2016**, *50* (17), 9061−9069.
(7) Niles, S. F.; Chacón-Patiño, M. L.; Chen, H.; McKenna, A. M.; Blakney, G. T.; Rodgers, R. P.; Marshall, A. G. Molecular-Level Characterization of Oil-Soluble Ketone/Aldehyde Photo-Oxidation Products by Fourier Transform Ion Cyclotron Resonance Mass Spectrometry Reveals Similarity Between Microcosm and Field Samples. *Environ. Sci. Technol.* **2019**, *53* (12), 6887−6894.
(8) Niles, S. F.; Chacón-Patiño, M. L.; Rodgers, R. P.; Marshall, A. G. Molecular Composition of Photooxidation Products Derived from Sulfur-Containing Compounds Isolated from Petroleum Samples. *Energy Fuels* **2020**, *34* (11), 14493−14504.
(9) Chacón-Patiño, M. L.; Niles, S. F.; Marshall, A. G.; Hendrickson, C. L.; Rodgers, R. P. Role of Molecular Structure in the Production of Water-Soluble Species by Photooxidation of Petroleum Compounds. *Environ. Sci. Technol.* **2020**, *54* (16), 9968−9979.
(10) King, S. M.; Leaf, P. A.; Olson, A. C.; Ray, P. Z.; Tarr, M. A. Photolytic and Photocatalytic Degradation of Surface Oil from the *Deepwater Horizon* Spill. *Chemosphere* **2014**, *95*, 415−422.
(11) Ray, P. Z.; Tarr, M. A. Solar Production of Singlet Oxygen from Crude Oil Films on Water. *J. Photochem. Photobiol., A* **2014**, *286*, 22−28.
(12) Garrett, R. M.; Pickering, I. J.; Haith, C. E.; Prince, R. C. Photooxidation of Crude Oils. *Environ. Sci. Technol.* **1998**, *32* (23), 3719−3723.
(13) Lee, R. F. Photo-Oxidation and Photo-Toxicity of Crude and Refined Oils. *Spill Sci. Technol. Bull.* **2003**, *8* (2), 157−162.
(14) Chacón-Patiño, M. L.; Rowland, S. M.; Rodgers, R. P. Advances in Asphaltene Petroleomics. Part 1: Asphaltenes Are Composed of Abundant Island and Archipelago Structural Motifs. *Energy Fuels* **2017**, *31* (12), 13509−13518.
(15) Chacón-Patiño, M. L.; Rowland, S. M.; Rodgers, R. P. Advances in Asphaltene Petroleomics. Part 2: Selective Separation Method That Reveals Fractions Enriched in Island and Archipelago Structural Motifs by Mass Spectrometry. *Energy Fuels* **2018**, *32* (1), 314−328.
(16) Chacón-Patiño, M. L.; Rowland, S. M.; Rodgers, R. P. Advances in Asphaltene Petroleomics. Part 3. Dominance of Island or Archipelago Structural Motif Is Sample Dependent. *Energy Fuels* **2018**, *32* (9), 9106−9120.
(17) Niles, S. F.; Chacón-Patiño, M. L.; Smith, D. F.; Rodgers, R. P.; Marshall, A. G. Comprehensive Compositional and Structural Comparison of Coal and Petroleum Asphaltenes Based on Extrography Fractionation Coupled with Fourier Transform Ion Cyclotron Resonance MS and MS/MS Analysis. *Energy Fuels* **2020**, *34* (2), 1492−1505.
(18) Niles, S. F.; Chacón-Patiño, M. L.; Putnam, S. P.; Rodgers, R. P.; Marshall, A. G. Characterization of an Asphalt Binder and Photoproducts by Fourier Transform Ion Cyclotron Resonance Mass Spectrometry Reveals Abundant Water-Soluble Hydrocarbons. *Environ. Sci. Technol.* **2020**, *54* (14), 8830−8836.
(19) Payne, J. R.; Phillips, C. R. Photochemistry of Petroleum in Water. *Environ. Sci. Technol.* **1985**, *19* (7), 569−579.
(20) Skold, C. N.; Schlessinger, R. H. The Reaction of Singlet Oxygen with a Simple Thiophene. *Tetrahedron Lett.* **1970**, *11* (10), 791−794.
(21) Larson, R. A.; Hunt, L. L. Photooxidation of a Refined Petroleum Oil: Inhibition By β-Carotene and Role of Singlet Oxygen. *Photochem. Photobiol.* **1978**, *28* (4−5), 553−555.
(22) Ehrhardt, M. G.; Bícego, M. C.; Weber, R. R. Photo-Oxidation of 1-Methylnaphthalene Dissolved in Seawater and Exposed to Sunlight under Quasi-Environmental Conditions. *J. Photochem. Photobiol., A* **1997**, *108*, 253−259.
(23) Liang, J. J.; Gu, C. L.; Kacher, M. L.; Foote, C. S. Chemistry of Singlet Oxygen. 45. Mechanism of the Photooxidation of Sulfides. *J. Am. Chem. Soc.* **1983**, *105* (14), 4717−4721.
(24) Nicodem, D. E.; Fernandes, M. C. Z.; Guedes, C. L. B. B.; Correa, R. J. Photochemical Processes and the Environmental Impact of Petroleum Spills. *Biogeochemistry* **1997**, *39* (2), 121−138.
(25) Thingstad, T.; Pengerud, B. The Formation of "Chocolate Mousse" from Statfjord Crude Oil and Seawater. *Mar. Pollut. Bull.* **1983**, *14* (6), 214−216.
(26) Rontani, J. F.; Giral, P. J. Significance of Photosensitized Oxidation of Alkanes During the Photochemical Degradation of Petroleum Hydrocarbon Fractions in Seawater. *Int. J. Environ. Anal. Chem.* **1990**, *42* (1−4), 61−68.
(27) Putman, J. C.; Rowland, S. M.; Podgorski, D. C.; Robbins, W. K.; Rodgers, R. P. Dual-Column Aromatic Ring Class Separation with Improved Universal Detection across Mobile-Phase Gradients via Eluate Dilution. *Energy Fuels* **2017**, *31*, 12064−12071.
(28) Boduszynski, M. M. Composition of Heavy Petroleums. 2. Molecular Characterization. *Energy Fuels* **1988**, *2* (5), 597−613.
(29) Dittmar, T.; Koch, B.; Hertkorn, N.; Kattner, G. A Simple and Efficient Method for the Solid-Phase Extraction of Dissolved Organic Matter (SPE-DOM) from Seawater. *Limnol. Oceanogr.: Methods* **2008**, *6* (6), 230−235.
(30) Kaiser, N. K.; Quinn, J. P.; Blakney, G. T.; Hendrickson, C. L.; Marshall, A. G. A Novel 9.4 T FTICR Mass Spectrometer with Improved Sensitivity, Mass Resolution, and Mass Range. *J. Am. Soc. Mass Spectrom.* **2011**, *22* (8), 1343−1351.
(31) Podgorski, D. C.; Corilo, Y. E.; Nyadong, L.; Lobodin, V. V.; Bythell, B. J.; Robbins, W. K.; McKenna, A. M.; Marshall, A. G.; Rodgers, R. P. Heavy Petroleum Composition. 5. Compositional and Structural Continuum of Petroleum Revealed. *Energy Fuels* **2013**, *27* (3), 1268−1276.
(32) Lobodin, V. V.; Juyal, P.; McKenna, A. M.; Rodgers, R. P.; Marshall, A. G. Tetramethylammonium Hydroxide as a Reagent for Complex Mixture Analysis by Negative Ion Electrospray Ionization Mass Spectrometry. *Anal. Chem.* **2013**, *85* (16), 7803−7808.
(33) Smith, D. F.; Podgorski, D. C.; Rodgers, R. P.; Blakney, G. T.; Hendrickson, C. L. 21 T FT-ICR Mass Spectrometer for Ultrahigh-Resolution Analysis of Complex Organic Mixtures. *Anal. Chem.* **2018**, *90* (3), 2041−2047.
(34) Blakney, G. T.; Hendrickson, C. L.; Marshall, A. G. Predator Data Station : A Fast Data Acquisition System for Advanced FT-ICR MS Experiments. *Int. J. Mass Spectrom.* **2011**, *306* (2−3), 246−252.
(35) Corilo, Y. E. *PetroOrg Software*; Omics LLC: Tallahassee, FL, 2014.
(36) Hsu, C. S.; Lobodin, V. V.; Rodgers, R. P.; McKenna, A. M.; Marshall, A. G. Compositional Boundaries for Fossil Hydrocarbons. *Energy Fuels* **2011**, *25* (5), 2174−2178.
(37) Zito, P.; Podgorski, D. C.; Bartges, T.; Guillemette, F.; Roebuck, J. A.; Spencer, R. G. M.; Rodgers, R. P.; Tarr, M. A. Sunlight-Induced Molecular Progression of Oil into Oxidized Oil Soluble Species, Interfacial Material, and Dissolved Organic Matter. *Energy Fuels* **2020**, *34* (4), 4721−4726.

https://doi.org/10.1021/acs.energyfuels.1c02373
Energy Fuels XXXX, XXX, XXX−XXX